UNIVERSITY OF HELSINKI REPORT SERIES IN PHYSICS

HU-P-D182

NEW COMPUTATIONAL APPROACHES FOR INELASTIC X-RAY SCATTERING

Arto Sakko

Division of Materials Physics
Department of Physics
Faculty of Science
University of Helsinki
Helsinki, Finland

ACADEMIC DISSERTATION

To be presented, with the permission of
the Faculty of Science of the University of Helsinki,
for public criticism in Auditorium E204
of the Department of Physics (Physicum),
Gustaf Hällströmin katu 2a, on July 1st 2011 at 12:15

Helsinki 2011

Supervisor:

Prof. Keijo Hämäläinen
Department of Physics
University of Helsinki
Helsinki, Finland

Pre-examiners:

Prof. Tapio T. Rantala
Department of Physics
Tampere University of Technology
Tampere, Finland

Prof. Risto Nieminen
Department of Applied Physics
Aalto University School of Science and Technology
Espoo, Finland

Opponent:

Dr. Miguel A. L. Marques
Laboratoire de Physique de la Matière Condensée et Nanostructures
Université Claude Bernard Lyon 1 et CNRS
Villeurbanne, France

Custos:

Prof. Keijo Hämäläinen
Department of Physics
University of Helsinki
Helsinki, Finland

Report Series in Physics HU-P-D182
ISSN 0356-0961
ISBN 978-952-10-6881-2 (printed version)
ISBN 978-952-10-6882-9 (pdf version)
http://ethesis.helsinki.fi/
Helsinki University Print
Helsinki 2011

Preface

Many people have helped and supported me during the last years and it is a pleasure to acknowledge them for their invaluable contribution in this work. The work was carried out at the Division of Materials Physics at the University of Helsinki. I want to thank Prof. Keijo Hämäläinen for the supervision, encouragement and advices as well as for the possibility to work in such an inspiring research group. Dr. Aleksi Soininen was my most important source of information during the early stage of this work and I am deeply thankful to him for his help in guiding me to understand theoretical condensed matter physics. I would like to thank Prof. Angel Rubio, Dr. Christian Sternemann, Dr. Felix Lehmkühler, Dr. Mikko Hakala and Tuomas Pylkkänen for all the help and valuable discussions that had a big positive impact on this work. I am also thankful to Prof. Seppo Manninen for initially offering me the possibility to work at the x-ray laboratory and providing me the introduction to x-ray physics. I also thank Prof. Juhani Keinonen for the opportunity to work at the Department of Physics. The work was mainly funded by the Academy of Finland and the National Graduate School in Materials Physics. In addition some important research visits were funded by Jenny and Antti Wihuri Foundation, Vilho, Yrjö and Kalle Väisälä Foundation, DAAD, and the HPC-Europa2 programme.

I was fortunate to have an opportunity to collaborate with many skillful people also in other universities during my thesis work. The research visits in Dortmund and San Sebastián offered many memorable moments and I am grateful to my collaborators there for their warm hospitality. The workmates at the x-ray lab created a great working atmosphere and I am happy that I could work with such nice people there. I also want to thank my friends and my family for the support and encouraging. Most of all I thank Nanne who was my biggest source of encouragement and strength and who has always helped me understand what really matters in life.

A. Sakko: New computational approaches for inelastic x-ray scattering, University of Helsinki, 2011, 37 pages + appendices. University of Helsinki, Report Series in Physics, HU-P-D182.

Classification (INSPEC): A7870C, A7115, A7150
Keywords: inelastic x-ray scattering, density functional theory, time-dependent density functional theory

Abstract

Inelastic x-ray scattering spectroscopy is a versatile experimental technique for probing the electronic structure of materials. It provides a wealth of information on the sample's atomic-scale structure, but extracting this information from the experimental data can be challenging because there is no direct relation between the structure and the measured spectrum. Theoretical calculations can bridge this gap by explaining the structural origins of the spectral features. Reliable methods for modeling inelastic x-ray scattering require accurate electronic structure calculations. This work presents the development and implementation of new schemes for modeling the inelastic scattering of x-rays from non-periodic systems. The methods are based on density functional theory and are applicable for a wide variety of molecular materials. Applications are presented in this work for amorphous silicon monoxide and several gas phase systems. Valuable new information on their structure and properties could be extracted with the combination of experimental and computational methods.

List of publications

This thesis consists of an introductory part and five publications which are referred to using Roman numerals **I-V** throughout the text.

I **A. Sakko**, M. Hakala, J. A. Soininen, and K. Hämäläinen, *Density functional study of x-ray Raman scattering from aromatic hydrocarbons and polyfluorene* Physical Review B **76**, 205115 (2007).

II **A. Sakko**, C. Sternemann, Ch. J. Sahle, H. Sternemann, O. M. Feroughi, H. Conrad, F. Djurabekova, A. Hohl, G. T. Seidler, M. Tolan, and K. Hämäläinen, *Suboxide interface in disproportionating a-SiO studied by x-ray Raman scattering* Physical Review B **81**, 205317 (2010).

III **A. Sakko**, S. Galambosi, J. Inkinen, T. Pylkkänen, M. Hakala, S. Huotari, and K. Hämäläinen, *Inelastic x-ray scattering and vibrational effects at the K-edges of gaseous N_2, N_2O, and CO_2* Physical Chemistry Chemical Physics, doi: 10.1039/C1CP20295B (2011).

IV **A. Sakko**, A. Rubio, M. Hakala, and K. Hämäläinen, *Time-dependent density functional approach for the calculation of inelastic x-ray scattering spectra of molecules* Journal of Chemical Physics **133**, 174111 (2010).

V J. A. Bradley, **A. Sakko**, G. T. Seidler, A. Rubio, M. Hakala, K. Hämäläinen, G. Cooper, A. P. Hitchcock, K. Schlimmer, and K. P. Nagle, *Revisiting the Lyman-Birge-Hopfield Band of N_2* Physical Review A, accepted for publication (2011).

The author of this thesis is responsible for the theoretical work, code development, and electronic structure calculations presented in all papers. Molecular dynamics simulations in paper **II** were carried out by F. Djurabekova. The author introduced the scheme for extracting the suboxide contributions in that paper and performed the corresponding numerical analysis together with C. Sternemann. In paper **III** he was also involved in the interpretation and analysis of the experimental data. The author wrote the first versions of papers **I-IV** and for paper **V** he wrote the section concerning theoretical methods.

Contents

1 Introduction

Understanding the microscopic structure of materials and the ability to control it had a strong impact on technology and society in the 20th century. The knowledge of the underlying physics made it possible to design components and devices with characteristics tailored for a variety of applications. The focus of the research has shifted towards even smaller length and time scales, such as nanotechnological applications and attosecond physics. Large-scale experimental facilities have enabled new kinds of measurements and constantly provide interesting scientific findings. Also the rapid development of computational physics has contributed to the improved understanding of many complicated phenomena in the atomic scale. Increased computational power and the development of efficient electronic structure calculation methods now enable accurate simulation of the properties of condensed matter systems. Combination of the state-of-the-art calculations and experiments at the large-scale facilities can provide the most comprehensive understanding of the materials, and the development of new computational methods for this purpose is thus essential.

X-rays are widely used in materials research due to their appropriate wavelength that is comparable to the interatomic spacing. X-ray absorption and emission spectroscopies are frequently used techniques for element-specific studies. This work, however, focuses on the nonresonant inelastic x-ray scattering (NRIXS) technique whose potential in the structural studies has been revealed relatively lately. [1] For a long time the low inelastic scattering cross section hindered experimental data collection with sufficient statistical accuracy. This condition has changed with the emergence of third generation synchrotron radiation facilities and crystal spectrometers that enable efficient data collection. [2, 3] New kinds of experiments have become possible and the applicability of NRIXS has been extended to the study of new materials, elements, and experimental conditions. [4–7]

Concerning its applications, NRIXS bears similarity to x-ray absorption spectroscopy (XAS) which is a widely used technique for studying the local atomic scale structure of various materials. [8] At small scattering angles NRIXS can approximately yield the x-ray absorption spectrum but the scattering angle dependence reveals also additional information. [9] Due to the different experimental requirements, NRIXS is applicable in many studies where the surface or saturation effects obscure the use of XAS. These advantageous features make NRIXS a favorable technique for the studies of various disordered materials. A good example is the microscopic structure of liquid water, where inelastic x-ray scattering with its bulk-sensitivity and high structure-sensitivity provides a very insightful experimental approach. [10–13] These studies have increased the knowledge of the complicated hydrogen bond network of molecular liquids and helped in understanding the x-ray absorption spectra of such systems. NRIXS also enables experiments at unusual conditions and it has been used in probing the mi-

croscopic changes during phase transitions at specific temperatures or at very high pressures. [14–16] The scattering angle dependence has been utilized in probing indirect band gaps of dielectrics and for studying the symmetry properties of electronic states. [17, 18] It has also been used in characterizing excitons. [19–21]

The wide applicability of inelastic x-ray scattering is well acknowledged now, but the analysis of the experimental data still requires effort and creativity. The challenge is to connect the features of the NRIXS spectrum to the material's structure or other property of interest. Unfortunately there is no direct and general relation between them, and even at the approximate level their connection may be complicated. The computational methods are invaluable in understanding the origins of the experimental features and thereby in establishing the structure-to-property relation. Schemes for calculating the NRIXS spectra have been developed for this purpose in the past, especially for crystalline and amorphous solids. [22–28] These studies have demonstrated the need for advanced calculation schemes that account for the electron-hole interactions. For molecular systems corresponding calculation schemes have been scarcer, partly because of the lack of experimental NRIXS studies on such systems until recent years. The necessary computational machinery of quantum chemistry has nevertheless been available for long time and has been utilized in analyzing the electron energy loss spectroscopy (EELS) data where the probed electronic transitions obey similar selection rules as in NRIXS. These calculations have often focused on individual transitions of small molecules and on the role of electronic correlation effects for the transition rates. [29–32] To interpret the experimental NRIXS spectra in terms of structural properties the computational methods that are applicable for wide energy ranges and for larger nanoscale systems are favorable. This work presents new methods for modeling the NRIXS spectra of molecular materials (systems consisting of up to hundreds of atoms) and demonstrates them in solving problems in materials science.

The structure of the thesis is as follows: In Section 2 an overview of the inelastic x-ray scattering technique is presented. The basic equations for the scattering cross section are given and NRIXS experiments are described. Section 3 reviews the theoretical foundations of the electronic structure theory and in Section 4 the calculations of this work are described. Some demonstrative examples of the computational methods presented in this work are given. Section 5 gives a summary of the papers that are included in this thesis. In addition to the new computational methods, the papers present their applications and in particular they include a study of the microscopic structure of disproportionating amorphous silicon monoxide and of the excited state properties of dinitrogen molecule.

Throughout this thesis, atomic units (a.u.) are employed in the formulae. Numerical values are given in SI units, electron volts, or Ångströms.

2 Inelastic x-ray scattering

Understanding how the electromagnetic radiation interacts with matter is the basic requirement for describing the inelastic x-ray scattering (IXS) process. When photons pass through a material and interact with its electrons and nuclei, they can be absorbed or scattered elastically or inelastically. The probabilities of these processes depend strongly on the wavelength of the light as well as on the structure of the material. Elastic scattering is employed e.g. in x-ray diffraction for the determination of crystalline structures. Photoabsorption and elastic scattering are the dominant processes in the energy ranges from infrared to soft x-ray energies, but at hard x-ray energies (above ∼50 keV) they give way to inelastic x-ray scattering.

Using spectroscopic techniques, such as IXS, one can observe that the elementary excitations often occur at certain material-specific energies. For example, infrared absorption is especially strong at the wavelengths that correspond to the material's vibrational or phonon energies. A similar phenomenon is observed in optical and x-ray photoabsorption spectroscopies where the resonances are caused by excitations of the electrons in the material. In the IXS process part of the incident photon's energy is transferred to the sample, and the scattering is most probable when the energy transfer is close to the characteristic excitation energies of the material. Theoretical understanding of the scattering process is necessary for connecting the scattering cross section with the electronic structure of the sample material. This chapter gives a brief overview to the inelastic x-ray scattering technique and introduces the basic equations that are necessary to understand this relation.

2.1 Scattering cross section

Inelastic x-ray scattering is a photon-in-photon-out process where the properties of the photon (energy, momentum, and polarization state) can change. In the IXS spectroscopy the energies of the incident and scattered x-rays (ω_1 and ω_2, respectively) are usually much larger than the energy transfer $\omega = \omega_1 - \omega_2$. By varying the scattering angle, the momentum transfer $\mathbf{q} = \mathbf{q}_1 - \mathbf{q}_2$ can be chosen separately from the energy transfer. This freedom makes it possible to study e.g. the dispersion curves of the observed excitations.

Theoretical description of the scattering of x-rays from elementary excitations requires quantum mechanical treatment of the process. Interaction of the electromagnetic radiation with materials can be described using the minimal substitution which gives an additional interaction term in the Hamiltonian of the scattering system. If the relativistic effects and the scattering from nuclei are neglected, this term is

$$\mathbf{H}_{\text{int}} = \sum_j \left(\frac{1}{2} \mathbf{A}(\mathbf{r}_j, t) \cdot \mathbf{A}(\mathbf{r}_j, t) + \mathbf{p}_j \cdot \mathbf{A}(\mathbf{r}_j, t) \right) \tag{1}$$

where $\mathbf{A}(\mathbf{r}, t)$ is the operator of the vector potential of the electromagnetic field and $\mathbf{r}_j$ and $\mathbf{p}_j$ are the position and momentum operators of the electron j, respectively. [33] The interaction causes the electronic system to undergo transitions between the eigenstates of its Hamiltonian, i.e. it induces elementary excitations. Applying the first-order time-dependent perturbation theory to calculate the transition probabilities for scattering yields the double differential scattering cross section to the solid angle element $d\Omega_2$:

$$\frac{d^2\sigma}{d\Omega d\omega_2} = r_0^2 \left(\frac{\omega_2}{\omega_1}\right) |\mathbf{e}_1 \cdot \mathbf{e}_2^*|^2 \sum_{I,F} \rho_I \left| \langle F| \sum_j e^{i\mathbf{q}\cdot\mathbf{r}_j} |I\rangle \right|^2 \delta(E_F - E_I - \omega). \quad (2)$$

Here I and F denote the initial and the final many-particle states of the sample material, respectively, and E_I and E_F are their total energies. $\mathbf{e}_1$ and $\mathbf{e}_2$ are the unit polarization vectors of the incident and scattered photons, respectively, r_0 is the classical electron radius, and ρ_I are the statistical weights for the involved initial states. The second-order perturbation theory would give extra terms in the cross section that describe e.g. resonant inelastic scattering. [33] The contribution of resonant scattering is nevertheless small if the incident energy is far from the binding energies of the electrons of the material. This is the case throughout this work and therefore the resonant terms are omitted.

2.2 Dynamic structure factor

The double differential cross section (Eq. 2) is proportional to the dynamic structure factor

$$S(\mathbf{q}, \omega) = \sum_{I,F} \rho_I |\langle F| \sum_j e^{i\mathbf{q}\cdot\mathbf{r}_j} |I\rangle|^2 \delta(E_F - E_I - \omega), \quad (3)$$

which is a central function in NRIXS and thereby in this work. It depends only on the electronic and structural properties of the material and not on the experimental setup. In particular it is independent of the energy of the incident x-rays. The behaviour of the dynamic structure factor at different energy transfers is illustrated in Fig. 1 that shows how it reflects the various elementary excitations at their characteristic energies. The momentum transfer dependence of $S(\mathbf{q}, \omega)$ gives more specific information on the nature of the excitations. It can be employed to study their symmetry properties and to probe the dispersion curves of plasmons and phonons. At high values of $\mathbf{q}$ and ω the broad Compton scattering feature reflects the momentum distribution of electrons in the sample material. [34] Historically, its finite width was the first experimental proof of the applicability of Fermi-Dirac statistics for conduction electrons. [35]

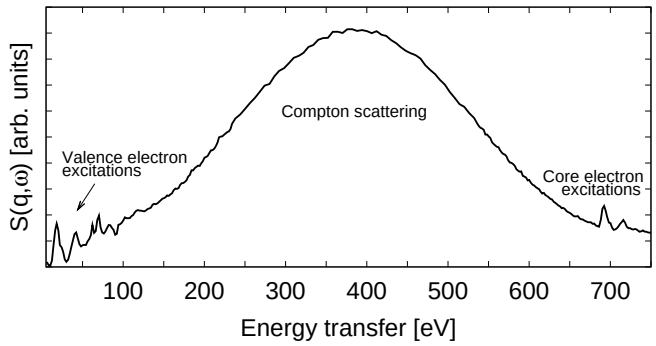

Figure 1: Experimental NRIXS spectrum of LiF at $q \approx 10$ Å^{-1} showing various electronic excitations at the different energy transfers. The spectrum was originally presented in Ref. 19.

Dynamic structure factor is also closely related to several important linear response functions of the sample material. Van Hove derived its connection to charge density fluctuations,

$$S(\mathbf{q},\omega) = \frac{1}{2\pi}\int d^3\mathbf{r}\int d^3\mathbf{r}'\int dt e^{i\mathbf{q}\cdot\mathbf{r}}e^{-i\omega t}\langle\rho(\mathbf{r}'-\mathbf{r},t)\rho(\mathbf{r}',0)\rangle, \tag{4}$$

where the Fourier transformed statistical expectation value is the density correlation function. [36] Using the fluctuation-dissipation theorem [37] the charge density correlations can be connected to the dielectric properties of the material, leading to the important relation

$$S(\mathbf{q},\omega) = \frac{-q^2}{4\pi^2 n}\mathrm{Im}\left[\frac{1}{\varepsilon_M(\mathbf{q},\omega)}\right], \tag{5}$$

where n is the average electron density of the system and ε_M its macroscopic dielectric function. Dynamic structure factor is thus related very closely to the optical and electrical properties of the materials and NRIXS can be used to study these bulk sensitively. Also the propagation of fast charged particles in materials can be described by the dielectric function and thus by the NRIXS energy loss spectrum. [38–41]

NRIXS experiments are mainly carried out at third generation synchrotron radiation facilities that provide sufficiently intense x-ray beams. Although one would like to determine $S(\mathbf{q},\omega)$ at the optimal energy and momentum resolution together with high statistical accuracy, these requirements are often conflicting and compromises between them have to be made. In typical NRIXS experiments the energy resolution is 0.3 - 1 eV and measurement times for a single spectrum are several hours. In order to use the limited beamtime efficiently it is often advantageous to focus only on the most relevant ranges of energy and momentum transfers. Calculations for $S(\mathbf{q},\omega)$ can help in preparing the experiment as they enable one to distinguish the most important spectral features, e.g. those that are the most structure-sensitive. It is also essential to understand how the energy and momentum resolution and the measurement times depend on the characteristics of the incident x-ray beam and on the performance of the spectrometer. In modern beamlines the x-rays are generated in the so-called insertion devices, i.e. undulators or wigglers. The energy of the incident photons can be tuned

and is usually 8 - 12 keV which provides appropriate penetration for bulk-sensitive studies and relieves the requirement for placing the sample in vacuum. The scattered radiation is collected by crystal analyzers [2, 3] that reflect the x-rays of the desired wavelength to the detector. The wavelength and thus the photon energy is chosen using a suitable diffraction condition. The NRIXS energy loss spectrum is obtained usually by recording the intensity at the detector when the analyzer energy is kept fixed and the incident beam energy is varied.

NRIXS experiments are routinely performed e.g. at the European Synchrotron Radiation Facility (ESRF, France), Advanced Photon Source (USA), and SPring-8 (Japan). There are also ongoing or proposed projects for building NRIXS-applicable beamlines at least in Soleil (France), PETRA-III (Germany), and Diamond (U.K.). Furthermore, one of the flagship projects of the ESRF Upgrade program is a dedicated beamline for electronic excitations that will enable microfocus experiments and increased flux for NRIXS studies. In addition to this development and the emerging applications at the third generation synchrotron radiation facilities, the free electron lasers operating at the hard x-ray regime will soon enable new kinds of experiments, such as nonlinear and time-resolved x-ray spectroscopy. New computational methods for these processes will be needed. [42, 43]

3 Electronic structure theory

The proper treatment of the inelastic x-ray scattering process requires that both the ground and the excited state electronic structures are characterized accurately. The electronic structure calculations in this work start from the nonrelativistic Hamiltonian

$$H = -\sum_J \frac{\nabla_J^2}{2M_J} - \sum_i \frac{\nabla_i^2}{2} + \sum_{i<i'} \frac{1}{|\mathbf{r}_i - \mathbf{r}_{i'}|} - \sum_{iJ} \frac{Z_J}{|\mathbf{r}_i - \mathbf{R}_J|} + \sum_{J<J'} \frac{Z_J Z_{J'}}{|\mathbf{R}_J - \mathbf{R}_{J'}|}, \quad (6)$$

where $\mathbf{R}_J$, Z_J, and M_J are the coordinates, atomic numbers, and the masses of the nuclei J, respectively, and $\mathbf{r}_i$ are the coordinates of the electrons i in the system. The solutions of the Schrödinger equation $H|\Psi\rangle = E|\Psi\rangle$, i.e. the many-particle states that also appear in Eq. 3, yield all physical observables and fundamental properties of the materials. Solving this equation is a formidable task and the full solution is only possible for very small systems. A basic approximation to facilitate the calculation is the separation of the fast motion of the electrons from the slower dynamics of the nuclei, which leads to individual Schrödinger equations for both parts. Nevertheless the calculation of the electronic equation still remains complicated and the most accurate methods for solving it, e.g. configuration interaction and coupled clusters, are the computationally heaviest ones. Density functional theory (DFT) provides calculation schemes that are much less expensive but nevertheless often very accurate. Its

time-dependent extension also introduces well justified methods for the excited state calculations.

3.1 Separating the electronic and nuclear dynamics

The Schrödinger equation for the many-body wavefunctions depends on both the electronic and nuclear coordinates, which makes its calculation complicated. In the Born-Oppenheimer approximation (BOA) the wavefunction is separated into electronic and nuclear parts and reads

$$\Psi(\mathbf{r},\mathbf{R}) = \Phi(\mathbf{r};\mathbf{R})\chi(\mathbf{R}), \tag{7}$$

where Φ and χ are the electronic and nuclear wavefunctions, and $\mathbf{r}$ and $\mathbf{R}$ are the sets of the electronic and nuclear coordinates, respectively. [44] For each configuration $\mathbf{R}$ one can write an electronic Schrödinger equation

$$H_e(\mathbf{r};\mathbf{R})\Phi(\mathbf{r};\mathbf{R}) = V(\mathbf{R})\Phi(\mathbf{r};\mathbf{R}), \tag{8}$$

where the electronic Hamiltonian H_e is chosen to include all terms of Eq. 6 except for the nuclear kinetic energy operator. The eigenvalues $V(\mathbf{R})$ provide the potential energy surfaces (PESs) which determine the nuclear dynamics. Applying the Hamiltonian (Eq. 6) to the ansatz of Eq. 7 and ignoring the effect of the nuclear kinetic operator on the electronic wavefunctions yields individual nuclear Schrödinger equations for each PES:

$$\left[-\sum_J \frac{\nabla_J^2}{2M_J} + V(\mathbf{R})\right]\chi(\mathbf{R}) = E\chi(\mathbf{R}). \tag{9}$$

Cuts through some calculated[1] potential energy surfaces for N_2O and H_2O molecules are shown in Fig. 2. Born-Oppenheimer approximation is valid if the PESs are sufficiently separated in energy. For more accurate calculations one should replace Eq. 7 by the general ansatz $\Psi(\mathbf{r},\mathbf{R}) = \sum_k \Phi_k(\mathbf{r};\mathbf{R})\chi_k(\mathbf{R})$, where k denotes the electronic states. This approach leads to a set of coupled nuclear Schrödinger equations and more complicated calculations. [45]

In order to solve Eq. 9 one needs to know the value of the PES at all possible configurations. The equation also involves a significant number of variables already for small molecules, i.e. $3N_{at}$, where N_{at} is the number of atoms. Often it is sufficient to study the nuclear dynamics only in the vicinity of the minimum of the PES, where the probability to find the nuclei is highest. The problem simplifies considerably by employing the harmonic approximation for the PES in this region and by introducing the normal coordinates in place of the nuclear coordinates. [46] The normal coordinates Q_m represent the displacements of the nuclei from the minimum of the PES and they (as well as the vibrational frequencies ω_m) can be found by diagonalizing the Hessian

[1] The calculation method is described in Sect. 4.1.

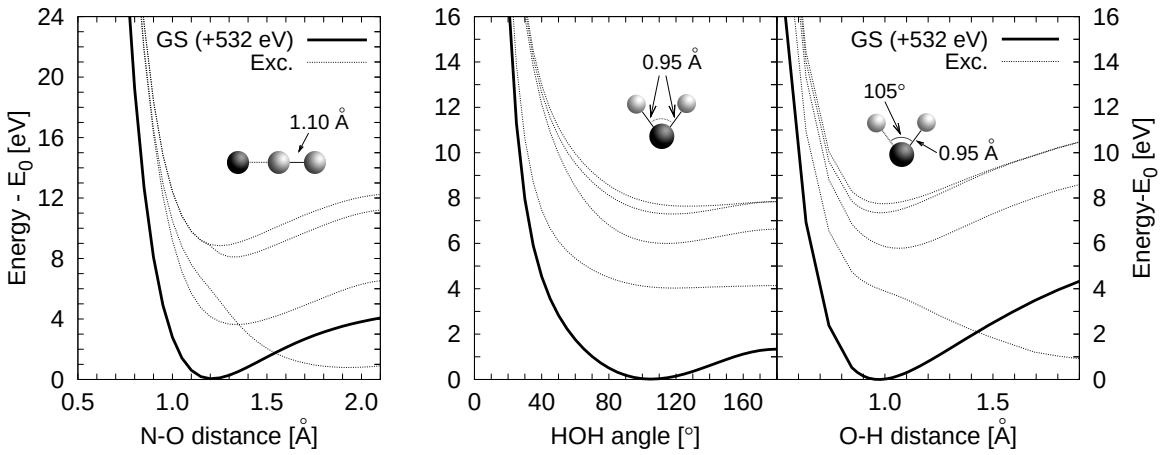

Figure 2: Calculated ground (GS) and first few core-excited (Exc.) state potential energy surfaces of (left) N_2O and of (right) H_2O. The value for E_0 is chosen in such a way that the shown ground state curve has a minimum at 0 eV.

matrix of the PES at its minimum. The normal mode approach transforms the original differential equation of $3N_{at}$ variables to $M = 3N_{at} - 6$ independent single-variable differential equations[2] whose solutions ψ_m are the harmonic oscillator eigenstates. The nuclear wavefunction then reads

$$\chi(\mathbf{R}) \equiv \chi(\mathbf{Q}) = \prod_{m=1}^{M} \psi_m(Q_m) \tag{10}$$

and the corresponding energy is $\sum_{m=1}^{M} \omega_m(\frac{1}{2}+n_m)$, where n_m is the vibrational quantum number for the m^{th} mode. [47]

3.2 Ground state electronic structure

The ground state electronic structure is the lowest-energy solution of Eq. 8 that is consistent with the Pauli exclusion principle. The electronic wavefunction depends on $3N$ electronic coordinates (plus the spin variables, which are omitted here for simplicity), where N is the number of electrons in the system. Many electronic structure calculation methods, e.g. Hartree-Fock and configuration interaction, are based on finding an approximation for the many-particle wavefunction that can be expressed as a linear combination of Slater determinants. [48] Another approach is to focus on the electronic Green's functions instead of the wavefunction. [49, 50] In DFT one in turn focuses on the electronic density and this method is used in this work. DFT bases

[2] $M = 3N_{at} - 5$ for linear molecules

on the Hohenberg-Kohn theorems proving that in addition to the many-particle wavefunction, all observable properties of a material can be derived also from its ground state electronic density which can be determined by variationally minimizing the total energy. [51] The practical DFT scheme was developed by Kohn and Sham [52] who wrote the electronic density in terms of single-particle orbitals ($\rho(\mathbf{r}) = \sum_j |\phi_j(\mathbf{r})|^2$) that are solved from the Kohn-Sham (KS) equations

$$\left[-\frac{1}{2}\nabla^2 + \int d^3\mathbf{r}' \frac{\rho(\mathbf{r}')}{|\mathbf{r}-\mathbf{r}'|} + V_{\mathrm{xc}}[\rho](\mathbf{r}) + V_{\mathrm{ext}}(\mathbf{r})\right]\phi_j(\mathbf{r}) = \varepsilon_j\phi_j(\mathbf{r}). \tag{11}$$

The four terms appearing in the Hamiltonian are the kinetic energy and the Hartree, exchange-correlation, and external potentials. The only unknown term is V_{xc} which includes the exchange (that is due to Pauli repulsion) and correlation (Coulombic interactions beyond the mean field Hartree potential) effects. The single-particle orbitals can be also used to construct a Slater determinant that approximates the true wavefunction.

The applicability of DFT in predicting the properties of different materials depends on two issues. First, the relation between the electronic density and the desired physical observables is not always known. For example, even though one would know the exact electronic density of the molecule, it is unknown how to deduce the electronic binding energies from it. The second issue is that the exchange-correlation potential is unknown and must be approximated. A widely used form for it is the local density approximation (LDA) whose value at a given point depends only on the electronic density at that point, and whose form is parametrized using the results for homogeneous electron gas. [52] Although the overall performance of LDA and its applicability in different problems is surprisingly good, it nevertheless has some drawbacks, e.g. it slightly overbinds molecules (it gives too high binding energies and too short bonds) and underestimates the total and ionization energies as well as the band gaps. [53, 54] Its deficiencies have been studied in detail during the last decades and significant effort has been dedicated to the development of more accurate functionals. In generalized gradient approximation V_{xc} at a given point also depends on the gradient of the density at that point. [55] Quite sophisticated orbital-dependent and semiempirical functionals are also frequently used and there are even functionals that are specifically designed for particular materials, e.g. liquid water. [56–59]

3.3 Electronic excitations

The electronic excitations that can take place in the material differ e.g. in their characteristic energy, degree of localization, number of electrons involved, and the way that the other electrons in the system respond to it. Accurate computational methods for simulating materials' properties have to take these into account. Static DFT only applies for time-independent external potentials and is, in principle, a ground state theory

but in some situations it can be applied also for predicting excited state properties. For example, the ionization potential of the system is the single-particle eigenvalue of the highest occupied orbital. [60] ΔKohn-Sham method for determining the electronic binding energies from total energy differences can be also justified. [53,61,62] Furthermore, Janak's theorem relates the single-particle eigenvalues with the variation of the total energy with respect to the occupation numbers, [63] yielding a transition state method for predicting the excitation energies of the electrons. [64]

Time-dependent perturbation theory provides well justified schemes for the excited state calculations. The basic idea is that when the system is perturbed by an external field, it is driven out of the ground state and its consequent behaviour then describes its excited state properties. When the perturbation is sufficiently weak, the induced effects can be expressed as a series expansion using response functions. An insightful case is the density response function $\chi(\mathbf{r}, \mathbf{r}', t)$ that is defined by the connection between the external potential $V_{\text{ext}}(\mathbf{r}, t)$ and the charge density change $\delta\rho_{\text{ext}}(\mathbf{r}, t)$ that the potential induces,

$$\delta\rho(\mathbf{r}, t) = \int_{-\infty}^{t} dt' \int d^3\mathbf{r}' \chi(\mathbf{r}, \mathbf{r}', t - t') V_{\text{ext}}(\mathbf{r}', t') + O(V_{\text{ext}}^2), \tag{12}$$

where $O(V_{\text{ext}}^2)$ includes all the nonlinear effects. Apart from some exceptional cases [65], the linear density response function in frequency space has poles at the exact excitation energies of the system. [66] Moreover, fluctuation-dissipation theorem [37] relates the dynamic structure factor and the density response function by the equation

$$S(\mathbf{q}, \omega) = -\frac{1}{\pi} \text{Im}\left[\chi(\mathbf{q}, -\mathbf{q}, \omega)\right] \tag{13}$$

and then Eq. 5 follows from the relation of the density response function and the macroscopic dielectric function. The connection means that in addition to the elementary excitations, $S(\mathbf{q}, \omega)$ at different energies and momenta contains information on the electronic density fluctuations at different time and length scales. [36,67]

Eqs. 12 and 13 show that the dynamic structure factor can be calculated if one can predict how the time-dependent electronic density behaves under the influence of external perturbations. Within the density functional framework the necessary extension to the time-dependent processes was presented by Runge and Gross. [68] They showed, analogously to the theorems of Hohenberg and Kohn, that the quantum mechanical system under an influence of time-dependent external fields can be described completely by the time-dependent electronic density and justified the time-dependent counterpart of Eq. 11:

$$\left[-\frac{1}{2}\nabla^2 + \int d^3\mathbf{r}' \frac{\rho(\mathbf{r}', t)}{|\mathbf{r} - \mathbf{r}'|} + V_{\text{xc}}[\rho](\mathbf{r}, t) + V_{\text{ext}}(\mathbf{r}, t)\right] \phi_j(\mathbf{r}, t) = i\frac{\partial\phi_j(\mathbf{r}, t)}{\partial t}. \tag{14}$$

Although the time-dependent DFT (TDDFT) and the linear response theory give the connection between the electronic density and the excitation energies, [69, 70] an approximation for the unknown exchange-correlation potential is still required. It is a

functional of the entire history of the density $\rho(\mathbf{r}, t)$ but usually its value at time t is calculated only from the density at that instant, i.e. an adiabatic approximation

$$V_{\mathrm{xc}}^{\mathrm{adiab}}[\rho](\mathbf{r}, t) \approx V_{\mathrm{xc}}[\rho(t)](\mathbf{r}) \tag{15}$$

is employed. Then the exchange-correlation potentials from static DFT can be used directly in the calculations. The most commonly used approximation is the adiabatic equivalent of the local density approximation (ALDA). It has provided excellent results for the photoabsorption spectra of molecules and nanoscale clusters as well as for the energy loss spectra of solids. [71,72] On the other hand, it has several deficiencies that restrict its applicability, including the locality, lack of memory, the wrong asymptotic behaviour, and the self-interaction error. [73–78] An important example is its failure to reliably predict band gaps and optical spectra of periodic systems. [50,66,79]. Moreover, ALDA predicts significantly too low core electron binding energies. [80] Despite some TDDFT-studies using sophisticated functionals have shown improved results, [78, 81] the calculations for inner-shell excitations are mostly carried out using static DFT with some suitable approximation for the core hole effects.

3.4 Vibrational transitions

As described in Sec. 3.1, the nuclear wavefunctions are the solutions of the Schrödinger equation (Eq. 9) where the relevant PES appears as the external potential. The wavefunctions are related to many important properties of the molecule, e.g. its vibrational frequencies. In the infrared absorption spectroscopy one can probe excitations where the electronic state of the molecule does not change but the nuclear part of the wavefunction undergoes a transition between two eigenstates of the same nuclear Hamiltonian, usually corresponding to the ground state PES. Infrared absorption peaks are then observed at the energies that correspond to the vibrational frequencies and the transition rates can be calculated from the nuclear wavefunctions. [82] Also in the electronic excitation spectra one can detect vibrational excitations, although in that case also the electronic state changes and the reason for the vibrational excitation is quite different. The electronic transition takes place extremely fast compared to the nuclear motion, which yields a sudden change in the external potential for the nuclei. Therefore the nuclear wavefunction, originally in an eigenstate of the ground state PES, ends up in a superposition of the eigenstates of the excited state PES. In other words the molecule has a finite probability to end up in a vibrationally excited state. This phenomenon causes side peaks (that is, vibrational fine structure) in the electronic excitation spectrum.

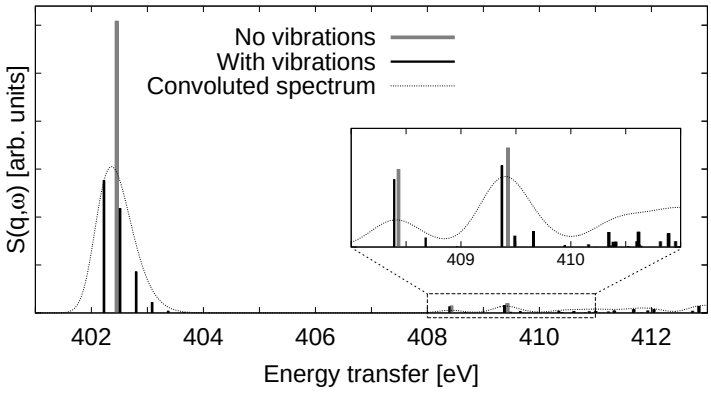

Figure 3: Calculated NRIXS spectrum (q=0.19 Å^{-1}) of N_2 molecule in the vicinity of the nitrogen K-edge with and without vibrational effects.

The intensities of the peaks in the fine structure depend on the nuclear wavefunctions participating in the transition and thereby reflect the shapes of the potential energy surfaces. The transition matrix element for the excitation is

$$\langle F|\hat{\mathbf{A}}|I\rangle = \int d\mathbf{R}[\chi^F(\mathbf{R})]^*\chi^I(\mathbf{R}) \int d\mathbf{r}[\Phi^F(\mathbf{r};\mathbf{R})]^*\hat{\mathbf{A}}\Phi^I(\mathbf{r};\mathbf{R}), \tag{16}$$

where $\hat{\mathbf{A}}$ is the transition operator ($\sum_j e^{i\mathbf{q}\cdot\mathbf{r}_j}$ in NRIXS). [83] Practical schemes for evaluating the transition rates often rely on the Condon approximation where the $\mathbf{R}$-dependence of the latter (electronic transition) integral of Eq. 16 is neglected and the integral is calculated only at the minimum energy configuration. The harmonic approximation for the PESs further simplifies the calculation as it facilitates the evaluation of the former (so-called Franck-Condon) integral of Eq. 16. [84,85] When the harmonic approximation is not valid, e.g. for dissociative states, alternative approaches must be used. [86,87] Figure 3 demonstrates the vibrational effect for the nitrogen K-edge NRIXS spectrum of N_2. It shows how the spectral intensity is distributed into several fine structure peaks. The convoluted spectrum then shows non-symmetric features.

4 Calculations

All electronic structure calculations in this work were carried out in the framework of density functional theory. A wide number of computer codes are available for DFT calculations nowadays. They differ in their implementations in several ways, and one important difference is the approach for expressing the single-particle orbitals. Typical choices are plane waves [88], localized basis functions [48], real space grids [89–92], and finite elements [93, 94]. Each approach has its advantages related e.g. to the numerical evaluation of the integrals and the parallelizability. In this work the StoBe-deMon computer code was employed for calculating the contribution of the inner shell excitations to the NRIXS spectrum (i.e. x-ray Raman scattering or XRS). [95, 96] It employs localized Gaussian basis functions to represent the single-particle orbitals.

Valence electron excitations were calculated with OCTOPUS computer code that uses a real space grid representation for the electronic states. [91, 97, 98]

4.1 Inner-shell excitations

Kohn-Sham DFT calculation provides a set of single-particle states that can be used to construct a Slater determinant which approximates the many-particle wavefunction. Within this approach the dynamic structure factor is

$$S(\mathbf{q},\omega) = \sum_f \left|\left\langle f|e^{i\mathbf{q}\cdot\mathbf{r}}|i\right\rangle\right|^2 \delta(\omega+\omega_i-\omega_f), \tag{17}$$

where i denotes the core-level orbital from which the excitation takes place and the sum includes all unoccupied single-particle states f. ω_i and ω_f are their eigenvalues, respectively.

Within Eq. 17 the excitation energies are obtained from the single-particle eigenvalue differences. The eigenvalues from a ground state calculation do not yield good transition energies, but they can be improved by taking into account that all electrons in the system respond to the presence of the core hole. [99] One possible way to estimate these relaxation effects is the Transition Potential Approximation (TPA). In this method the KS-equations are solved within the constraint that the occupancy of the excited inner-shell orbital is 0.5. [62] Other frequently used methods are the Z+1 approximation [100], ΔKohn-Sham method [53], and the final state rule [101]. Comparison of these methods for different systems has revealed that TPA works well in general, although for systems with strong excitonic effects the Z+1 method can be a better choice. [62, 102–105]

In STOBE-DEMON computer code the molecular orbitals are expressed using localized Gaussian-type basis functions centered at the nuclear coordinates $\mathbf{R}_j$ in the molecule:

$$\phi_n(\mathbf{r}) = \sum_j \zeta_{nj} P_j(\mathbf{r}-\mathbf{R}_j) e^{-\alpha_j(\mathbf{r}-\mathbf{R}_j)^2}, \tag{18}$$

where the polynomials P_j and the coefficients α_j depend on the chosen basis set. In this formulation the Kohn-Sham equation (Eq. 11) is solved for the coefficients ζ_{nj}. The quality of the basis set affects the accuracy of the solution for the electronic structure and thereby the desired observables. For the calculation of the near-edge XRS spectrum it is especially important to have a good representation of the electronic structure near the excited site. To achieve this, one can use specifically designed basis functions that enable improved description of the orbital relaxation effects. The delocalized continuum states can be also better represented by special diffuse basis sets. [96]

The localization of the core hole orbital requires additional consideration in the calculations when the system includes many atoms of the same element as the excited

one. This is because in that case there are multiple nearly degenerate core orbitals that are localized in the vicinity of all these atoms. If not somehow controlled, the core hole can then be centered at a wrong site. In the TPA calculations of this work the localization of the half-occupied core orbital at a specific atom site was enforced by using effective core potentials. [106, 107] In this method the core orbitals of the non-excited atoms of the same element as the excited one are removed from the problem and the other electrons experience a combined potential of the nucleus and the frozen core electrons, which is obtained from a predetermined atomic calculation. Only one core orbital remains, which ensures its proper localization.

The molecular orbitals that are represented using localized Gaussian basis functions can be transformed into spherical harmonic basis around the excited atom:

$$\phi_n(\mathbf{r}) = \sum_{l=0}^{\infty} \sum_{m=-l}^{+l} c_{lm}^n(r) Y_{lm}(\hat{\mathbf{r}}). \tag{19}$$

This is advantageous for the interpretation of the XRS spectrum, as demonstrated in the included papers **I** and **II** and in Ref. 13. In particular it enables one to decompose the matrix elements $\langle i|e^{i\mathbf{q}\cdot\mathbf{r}}|f\rangle$ and the ensuing XRS spectrum

i according to the transition channels; at low q only dipole transitions ($\Delta l = 1$) are observed but with increasing q also monopole, quadrupole, etc. transitions contribute.

ii with respect to the initial state; at the K-edge the initial state is almost completely of s-type and all the spectral intensity comes from the $l = 0$ component. At the L-edge the intensity in turn comes from the $l = 1$ component.

iii with respect to the final state; this decomposition describes the symmetry properties of the final states and yields a very insightful decomposition of the spectrum.

The spherical harmonic expansion of the orbitals also makes it possible to estimate the local density of states as

$$\mathrm{LDOS}(\omega) = \sum_f \sum_{l=0}^{\infty} \sum_{m=-l}^{+l} \int_0^R dr r^2 \left| c_{lm}^f(r) \right|^2 \delta(\omega - \omega_f), \tag{20}$$

where R was in this work chosen so that the integration regime contains $Z - 0.5$ electrons, Z being the atomic number of the excited site. The definition for LDOS is somewhat ambiguous, but one convenient feature of this expression is that Eq. 20 gives a well-defined density of states $\sum_f \delta(\omega - \omega_f)$ at the limit $R \to \infty$. It also enables one to separate the LDOS into its different angular momentum components in a straightforward way by including only the terms with the desired l. Moreover, the p-type LDOS can be decomposed into different cartesian directions by using the m-dependence of the terms. [13] Fig. 4 shows the angular momentum decomposition of LDOS for benzene

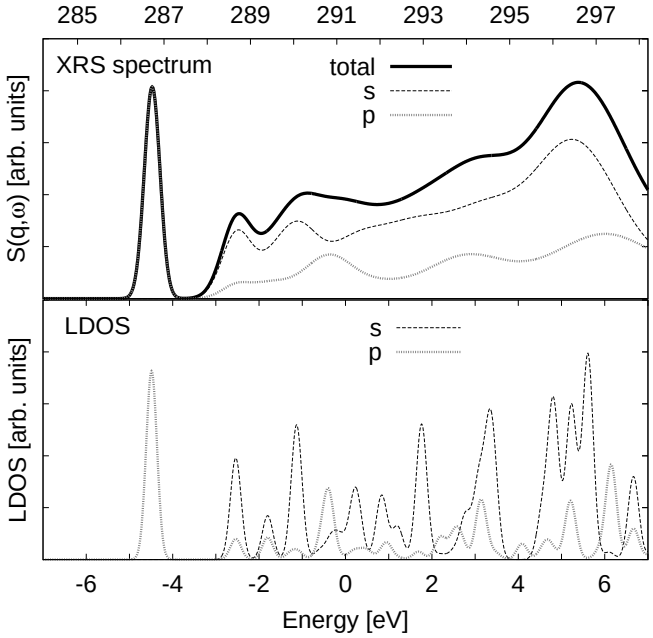

Figure 4: Calculated symmetry decomposition of the benzene XRS spectrum (at $q = 17$ Å^{-1}) to the s and p type final states and the comparison to the corresponding separation of the LDOS. The d-type (and higher) contribution in the spectrum is negligible and is therefore not shown here.

molecule in the vicinity of carbon atoms, and the decomposition of the corresponding carbon K-edge XRS spectrum into different final state components. Fig. 5 shows the relevant radial functions of the two orbitals that correspond to the strongest peak (at 286.7 eV) of the benzene spectrum. The initial state is very localized and completely of s-type character. The final state is a delocalized π^*-type orbital, yielding only p-type character with respect to the excited site. Its perpendicular orientation to the benzene ring is reflected in the very different p-type radial functions for $m = 0$ as compared with $m = \pm 1$.

4.2 Valence electron excitations

Whereas time-independent DFT within TPA has appeared to be a suitable method for calculating core-excitation spectra, it is not very applicable for valence excitations. This is partly because various initial states with similar energies contribute the spectrum in the same energy range and have different relaxation effects. The excitations can also couple with each other so that the single-excitation approximation is not valid. Time-dependent density functional theory provides a better starting point for such calculations. As discussed in Sect. 3.3, the ability to calculate the time-dependent electronic density with TDDFT means that also the density response function can be obtained. With an appropriate external potential, Eq. 12 can be solved for $\chi(\mathbf{r}, \mathbf{r}', t)$. In the time propagation method one uses $V_{ext}(\mathbf{r}, t) = I_0 e^{i\mathbf{q}\cdot\mathbf{r}}$ and calculates the induced charge density $\delta\rho(\mathbf{r}, t)$. Its Fourier transformation then gives $\chi(\mathbf{q}, -\mathbf{q}, \omega)$. In frequency space the analogous approach, i.e. studying the effect of a weak time-dependent perturbation on the system, leads to a Dyson-type equation for the density response

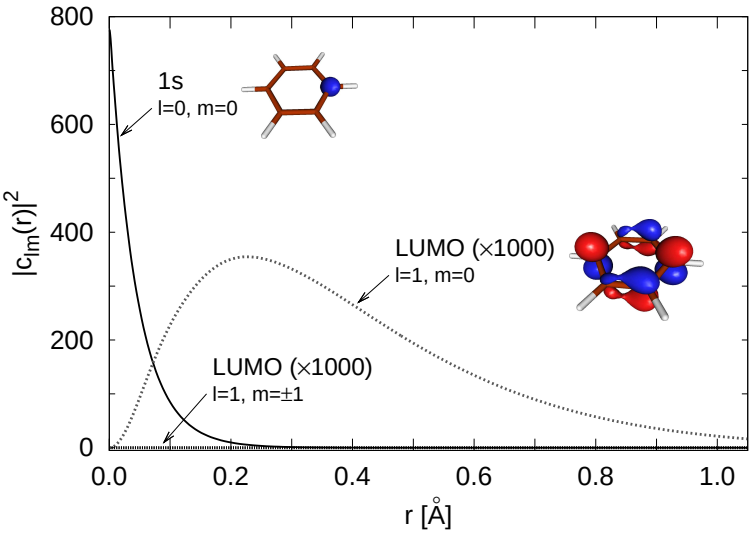

Figure 5: The relevant radial functions $c^n_{lm}(r)$ of the $1s$ orbital and of the lowest unoccupied molecular orbital (LUMO) of benzene with half occupied core hole.

function. [108] Casida formulated an efficient scheme for solving the response function for finite systems. [69]

The calculations were carried out using OCTOPUS computer code that enables TDDFT calculations for molecular systems. [91, 97] The single-particle orbitals are expressed in a numerical real space grid and the derivative operators are constructed by a finite differences method. The eigenvectors of the Kohn-Sham equation contain the values of the single-particle wavefunctions at the grid points. The time evolution of the system under the influence of an external field is determined by the Runge-Gross equations (Eq. 14), whose practical implementation is discussed in Ref. 109. An appealing feature of the real space grid approach is that the calculation parallelizes efficiently. [91] On the other hand, the remarkable number of degrees of freedom (grid points) can require significant computational cost. The number depends on the size of the system and on the distance between the grid points, which has to be small enough to accurately describe also the most localized states in the system. These are usually the core electrons, which however can be replaced by pseudopotentials. Within the pseudopotential approximation the electronic wave functions are different from the solutions of the original Kohn-Sham equations in the vicinity of the nuclei, but at the chemically more relevant spatial region between the atoms the difference vanishes. [110] To include the inner-shell electron dynamics in real-space calculations one would need a very small spacing or use of non-uniform grids [111, 112].

Since the time propagation and Casida's methods are based on the same theoretical framework, they, in principle, give same results. Nevertheless only very few direct comparisons of the results from the two methods exist in the literature. [113] This is partly because the two methods are applicable in different situations. Casida's method is an efficient scheme for calculating the bound-to-bound excitation energies and transition rates for small molecules. Time propagation scheme has a better scaling with

respect to the system size and it is therefore more suitable for large systems. [114, 115] It also enables, at least in principle, studies of the nonlinear response [116], combined electron-ion dynamics [117], ionization [118], nonequilibrium processes relevant in molecular electronics [119], and is also applicable in periodic systems. [120].

5 Summary of papers

This thesis includes five individual publications that present new computational methods (**papers I** and **IV**) and their applications (**papers II, III**, and **V**) in inelastic x-ray scattering spectroscopy. First of the developed methods is applicable for calculating the core-level excitation part of $S(\mathbf{q}, \omega)$, and the second one for the valence excitations. The methodological papers include benchmark test calculations, discussions about the underlying approximations and limitations of the methods, as well as suggestions for future improvements. The application papers report an analysis of the momentum transfer dependent XRS spectra of several molecules, provide new results concerning the structure of amorphous silicon monoxide, and present new insight into the excited state properties of N_2 molecule.

Paper I introduces a new computational method for calculating dynamic structure factor in the vicinity of x-ray absorption edges. It is based on the single-particle expression (Eq. 17) of the dynamic structure factor. The work presents calculations for aromatic hydrocarbon molecules and polyfluorene, showing good agreement with experimental data (Fig. 6). The results confirm the applicability of the developed method and the transition potential approximation based framework for momentum transfer dependent calculations. The paper also presents a scheme for expressing the single-particle states in spherical harmonic basis. This transformation enables one to decompose the transition matrix elements (and subsequently the XRS spectrum) into different transition channels providing new insight into the experimental spectrum. The method can be expected to work well for bound core-level transitions and to have applications in future XRS studies for molecular systems.

Paper II presents a study of the microscopic structure of disproportionating amorphous silicon monoxide which has advantageous properties for optical and semiconductor technology. In particular, since its atoms arrange in well separated domains of silicon and oxygen, the material contains a significant amount of silicon nanoclusters embedded in SiO_2. The size of these regions can be controlled experimentally by varying the annealing temperature T_A. [121] Moreover, at sufficiently high T_A Si nanocrystals form. In this paper the structure of the interface regions between the Si and SiO_2 domains was studied using XRS. Detailed understanding of the structure is important because further improvement of the material's properties (e.g. controlling the size distribution of the silicon nanocrystals) requires the understanding of how the bulk regions form and grow. Si/SiO_2 interfaces can also play an important role

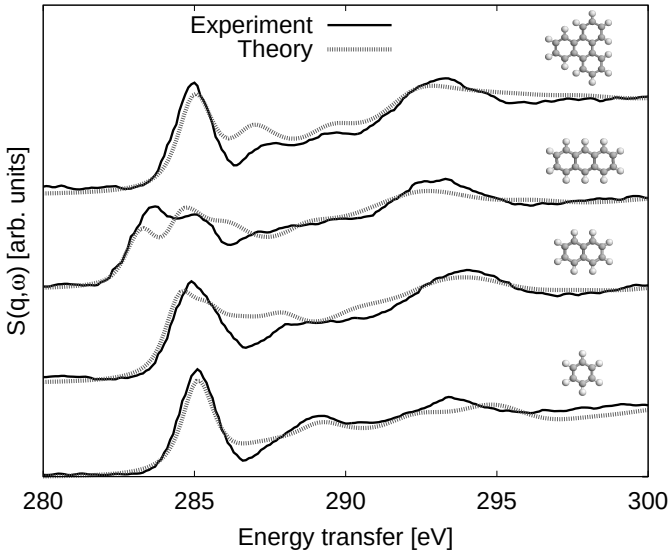

Figure 6: Calculated and experimental carbon K-edge energy loss spectrum of triphenylene, anthracene, naphthalene, and benzene (from top to bottom) at low momentum transfer.

for the optical properties of SiO_2-embedded silicon nanocrystals. [122] One aim of the study presented in **paper II** is the determination of the proportion of the Si atoms at the interfaces (or more specifically the amount of suboxidic Si atoms, i.e. silicons bonding with 1-3 oxygens). The approach that was taken in **paper II** uses NRIXS experiments, molecular dynamics simulations, and electronic structure calculations. The suboxide contribution of the experimental Si $L_{\mathrm{II,III}}$-edge spectrum was extracted using the annealing temperature dependence of the spectrum. The corresponding theoretical spectrum was calculated from the MD snapshots using the method of **paper I**. The content of the interfaces was extracted by finding the amount of suboxidic silicon atoms in the material that gives the best agreement between experimental and computational suboxide spectra. The resulting annealing temperature dependent suboxide proportion and the suboxide spectra for one anneling temperature (assuming binomial distribution of oxidation states) are shown in Fig. 7. The amount of suboxides and thereby the contribution of the interfaces was found to be larger than previously thought. Furthermore, the most remarkable structural changes take place at the annealing temperatures between 900°C and 1000°C.

Paper III presents one of the very first applications of NRIXS for gaseous samples. The experimental data is analyzed using the computational method of **paper I**. It also demonstrates how the molecular vibrations influence the experimental spectrum via simultaneous electronic-vibrational transitions. The paper shows how these vibrational effects can be modeled and dicusses more advanced schemes that could be used in the forthcoming NRIXS studies with improved energy resolution. The potential energy surfaces calculated with the transition potential approximation show good agreement with previous calculations presented in the literature. The calculations and the momentum transfer dependence of the observed excitations facilitate the assignment of

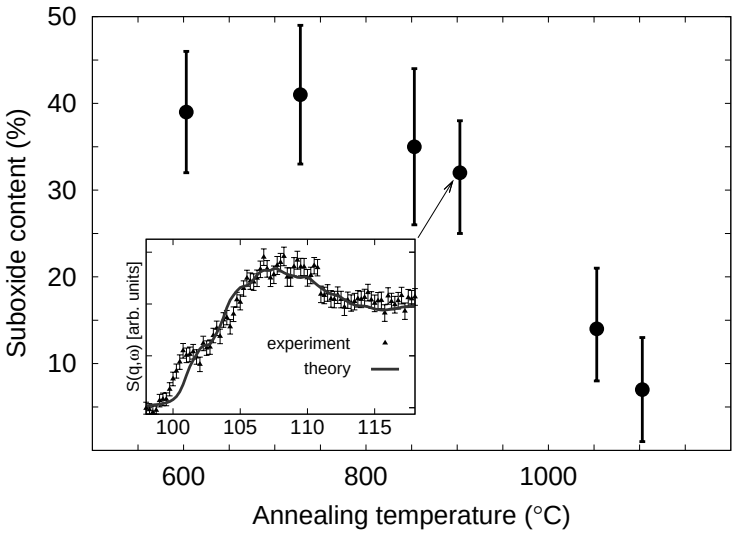

Figure 7: Extracted suboxide content of disproportionating amorphous silicon monoxide as a function of the annealing temperature. Inset shows the experimental and computational suboxide XRS spectra at q=9.85 Å^{-1} that were used to obtain the value for suboxide content at T_A=900°C.

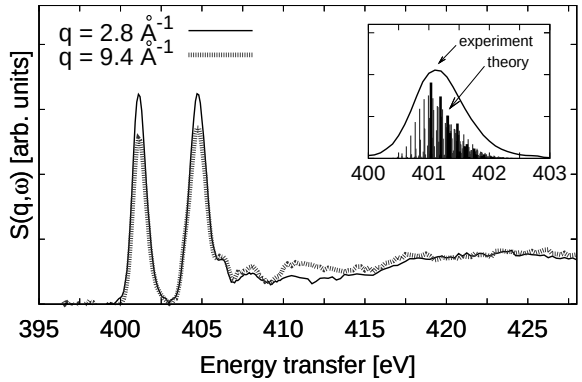

Figure 8: Experimental XRS spectrum of N_2O at the nitrogen K-edge for two indicated values of momentum transfer q. The inset shows the first peak (at low q) and the calculated vibrational fine structure. The sticks with different thicknesses correspond to the two electronic states that yield different vibrational lineshapes.

the spectral features with specific molecular orbitals. Figure 8 shows the experimental nitrogen K-edge spectra of N_2O and demonstrates how the vibrations affect its lowest-lying feature.

Paper IV introduces two novel TDDFT-based computational schemes for calculating the dynamic structure factor for non-periodic systems in the energy region of valence electron excitations. One of the schemes is based on the frequency space calculation of the density response function using Casida's method [69] and the second scheme uses the time propagation approach. [70] The paper shows how the time propagation approach yields the directionally averaged dynamic structure factor and how the calculated spectrum can be decomposed into different transition channels. The applicability and limitations of both methods are discussed in the paper and demonstrative calculations are presented for benzene and freon-13 molecule.

Paper V presents a study of the excited state properties of N_2 molecule and shows that the understanding of the so-called Lyman-Birge-Hopfield (LBH) transitions of its valence excitation spectrum has been incomplete. First reason is that at high q the previous EELS-derived transition rates have suffered from the violation of the

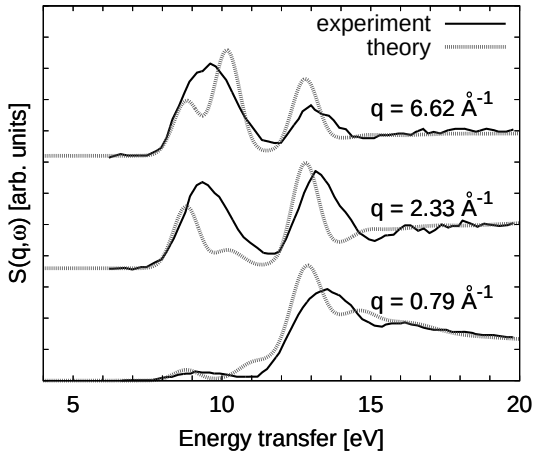

Figure 9: The calculated and experimental NRIXS spectrum of N_2 at the energy region of valence electron excitations. The Lyman-Birge-Hopfield feature is observed at $\sim$ 9 - 10 eV.

Born approximation that had not been taken into account. Secondly, we show that the dipole-forbidden LBH feature consists of two transitions with different momentum transfer dependencies, which is in contrast to the prior understanding. Experimental NRIXS and EELS spectra of gaseous nitrogen are analyzed using the computational method of **paper IV**. Our TDDFT calculations within the adiabatic local density approximation provide good agreement with the NRIXS data in the energy region of the LBH band (Fig. 9) and confirm the new interpretation of the energy loss spectrum of N_2.

6 Concluding remarks

This thesis presents new computational methods for the analysis of inelastic x-ray scattering data and their applications for obtaining new structural information on various materials. The development of such methods is important because the interpretation of the experimental spectra can be difficult without reliable theoretical approaches explaining the origin of the specific features in the data. The structural studies presented in this work demonstrate how the new methods give a deeper understanding of the studied materials.

There are several ways for continuing the present work and for improving the new methods further. Including the vibrational effects in a more general way would increase their applicability. This is desirable when the experimental energy resolution improves and enables high resolution studies for the vibrational fine structure. Further studies of the exchange and correlation effects on $S(\mathbf{q}, \omega)$ at the intermediate momentum transfer regime and the comparison to the previous EELS-related studies could provide interesting insight into the electronic excitations of molecules.

The methods developed in this work can play an important role in forthcoming NRIXS-studies where the momentum transfer dependence of the technique are utilized. They are straightforward to implement and examples of their use can be already found in Refs. 13, 16, 123 and 124, where the methods are applied to various alcohols, water, and clathrate hydrates.

Other Work

List of work by the author that is closely related to this thesis but not included in it.

1. H. Sternemann, C. Strenemann, G. T. Seidler, T. T. Fister, **A. Sakko**, and M. Tolan, *An extraction algorithm for core-level excitations in non-resonant inelastic x-ray scattering spectra*
   Journal of Synchrotron Radiation **15**, 162 (2008).

2. H. Conrad, F. Lehmkühler, C. Sternemann, **A. Sakko**, D. Paschek, L. Simonelli, S. Huotari, O. Feroughi, M. Tolan, and K. Hämäläinen, *Tetrahydrofuran clathrate hydrate formation*
   Physical Review Letters **103**, 218301 (2009).

3. Ch. J. Sahle, C. Sternemann, H. Conrad, A. Herdt, O. M. Feroughi, M. Tolan, A. Hohl, R. Wagner, D. Lützenkirchen-Hecht, R. Frahm, **A. Sakko**, and K. Hämäläinen, *Phase separation and nanocrystal formation in GeO*
   Applied Physics Letters **95**, 021910 (2009).

4. F. Lehmkühler, **A. Sakko**, C. Sternemann, M. Hakala, K. Nygård, Ch. J. Sahle, S. Galambosi, I. Steinke, S. Tiemeyer, A. Nyrow, T. Buslaps, D. Pontoni, M. Tolan, and K. Hämäläinen, *Anomalous energetics in tetrahydrofuran clathrate hydrate revealed by x-ray Compton scattering*
   Journal of Physical Chemistry Letters **1**, 2832 (2010).

5. O. M. Feroughi, C. Sternemann, Ch. J. Sahle, M. A. Schröer, H. Sternemann, H. Conrad, A. Hohl, G. T. Seidler, J. Bradley, T. T. Fister, M. Balasubramanian, **A. Sakko**, K. Pirkkalainen, K. Hämäläinen, and M. Tolan, *Phase separation and Si nanocrystal formation in bulk SiO studied by x-ray scattering*
   Applied Physics Letters **96**, 081912 (2010).

6. T. Pylkkänen, V. M. Giordano, J. Chervin, **A. Sakko**, M. Hakala, J. A. Soininen, K. Hämäläinen, G. Monaco, and S. Huotari, *Role of non-hydrogen-bonded molecules in the oxygen K-edge spectrum of ice*
   Journal of Physical Chemistry B **114**, 3804 (2010).

7. T. Pylkkänen, J. Lehtola, M. Hakala, **A. Sakko**, G. Monaco, S. Huotari, and K. Hämäläinen, *Universal signature of hydrogen bonding in the oxygen K-edge spectrum of alcohols*
   Journal of Physical Chemistry B **114**, 13076 (2010).

References

[1] W. Schülke, *Electron Dynamics by Inelastic X-ray Scattering* (Oxford University Press, Oxford, 2008).

[2] T. T. Fister, G. T. Seidler, L. Wharton, A. R. Battle, T. B. Ellis, J. O. Cross, W. T. Elam, A. T. Macrander, T. A. Tyson, and Q. Qian, *A multielement spectrometer for efficient measurement of the momentum transfer dependence of inelastic x-ray scattering*, Rev. Sci. Instrum. **77**, 063901 (2006).

[3] R. Verbeni, T. Pylkkänen, S. Huotari, L. Simonelli, G. Vankó, K. Martel, C. Henriquet, and G. Monaco, *Multiple-element spectrometer for non-resonant inelastic x-ray spectroscopy of electronic excitations*, J. Synchrotron Rad. **16**, 469 (2009).

[4] C. Sternemann, J. A. Soininen, S. Huotari, G. Vankó, R. A. Volmer, M. Secco, J. S. Tse, and M. Tolan, *X-ray Raman scattering at the L edges of elemental Na, Si, and the N edge of Ba in* Ba_8Si_{46}, Phys. Rev. B **72**, 035104 (2005).

[5] S. Galambosi, M. Knaapila, J. A. Soininen, K. Nygård, S. Huotari, F. Galbrecht, U. Scherf, A. P. Monkman, and K. Hämäläinen, *X-ray Raman scattering study of aligned polyfluorene*, Macromolecules **39**, 9261 (2006).

[6] M. Minzer, J. A. Bradley, R. Musgrave, G. T. Seidler, and A. Skilton, *A pressure cell for nonresonant inelastic x-ray scattering studies of gas phases.*, Rev. Sci. Instrum. **79**, 086101 (2008).

[7] T. T. Fister, D. D. Fong, J. A. Eastman, H. Iddir, P. Zapol, P. H. Fuoss, M. Balasubramanian, R. A. Gordon, K. R. Balasubramanian, and P. A. Salvador, *Total-reflection inelastic x-ray scattering from a 10-nm thick* $La_{0.6}Sr_{0.4}CoO_3$ *thin film*, Phys. Rev. Lett. **106**, 037401 (2011).

[8] J. Stöhr, *NEXAFS Spectroscopy* (Springer-Verlag, New York, 1992).

[9] U. Mizuno and Y. Ohmura, *Theory of x-ray Raman scattering*, J. Phys. Soc. Japan **22**, 445 (1967).

[10] U. Bergmann, P. Wernet, P. Glatzel, M. Cavalleri, L. G. M. Pettersson, A. Nilsson, and S. P. Cramer, *X-ray Raman spectroscopy at the oxygen K edge of water and ice: Implications on local structure models*, Phys. Rev. B **66**, 092107 (2002).

[11] P. Wernet, D. Nordlund, U. Bergmann, M. Cavalleri, M. Odelius, H. Ogasawara, L. A. Näslund, T. K. Hirsch, L. Ojamäe, P. Glatzel, L. G. M. Pettersson, and A. Nilsson, *The structure of the first coordination shell in liquid water*, Science **304**, 995 (2004).

[12] J. S. Tse, D. M. Shaw, D. D. Klug, S. Patchkovskii, G. Vankó, G. Monaco, and M. Krisch, *X-ray Raman spectroscopic study of water in the condensed phases*, Phys. Rev. Lett. **100**, 095502 (2008).

[13] T. Pylkkänen, V. M. Giordano, J. Chervin, A. Sakko, M. Hakala, J. A. Soininen, K. Hämäläinen, G. Monaco, and S. Huotari, *Role of non-hydrogen-bonded molecules in the oxygen K-edge spectrum of ice*, J. Phys. Chem. B **114**, 3804 (2010).

[14] W. L. Mao, H.-K. Mao, P. J. Eng, T. P. Trainor, M. Newville, C.-C. Kao, D. L. Heinz, J. Shu, Y. Meng, and R. J. Hemley, *Bonding changes in compressed superhard graphite*, Science **302**, 425 (2003).

[15] S. K. Lee, J.-F. Lin, Y. Q. Cai, N. Hiraoka, P. J. Eng, T. Okuchi, H. Mao, Y. Meng, M. Y. Hu, P. Chow, J. Shu, B. Li, H. Fukui, B. H. Lee, H. N. Kim, and C.-S. Yoo, *X-ray Raman scattering study of $MgSiO_3$ glass at high pressure: Implication for triclustered $MgSiO_3$ melt in Earth's mantle*, Proc. Nat. Aca. Sci. USA **105**, 7925 (2008).

[16] H. Conrad, F. Lehmkühler, C. Sternemann, A. Sakko, D. Paschek, L. Simonelli, S. Huotari, O. Feroughi, M. Tolan, and K. Hämäläinen, *Tetrahydrofuran clathrate hydrate formation*, Phys. Rev. Lett. **103**, 218301 (2009).

[17] W. A. Caliebe, J. A. Soininen, E. L. Shirley, C.-C. Kao, and K. Hämäläinen, *Dynamic structure factor of diamond and LiF measured using inelastic x-ray scattering*, Phys. Rev. Lett. **84**, 3907 (2000).

[18] J. A. Soininen, A. Mattila, J. J. Rehr, S. Galambosi, and K. Hämäläinen, *Experimental determination of the core-excited electron density of states*, J. Phys.: Cond. Matt. **18**, 7327 (2006).

[19] K. Hämäläinen, S. Galambosi, J. A. Soininen, E. L. Shirley, J.-P. Rueff, and A. Shukla, *Momentum dependence of fluorine K-edge core exciton in LiF*, Phys. Rev. B **65**, 155111 (2002).

[20] K. Yang, L. P. Chen, Y. Q. Cai, N. Hiraoka, S. Li, J. F. Zhao, D. W. Shen, H. F. Song, H. Tian, L. H. Bai, Z. H. Chen, Z. G. Shuai, and D. L. Feng, *Inelastic x-ray scattering study of exciton properties in an organic molecular crystal*, Phys. Rev. Lett. **98**, 036404 (2007).

[21] P. Abbamonte, T. Graber, J. P. Reed, S. Smadici, C. L. Yeh, A. Shukla, J. P. Rueff, and W. Ku, *Dynamical reconstruction of the exciton in LiF with inelastic x-ray scattering*, Proc. Nat. Aca. Sci. USA **105**, 12159 (2008).

[22] N. E. Maddocks, R. W. Godby, and R. J. Needs, *Bandstructure effects in the dynamic response of aluminium*, Europhys. Lett. **27**, 681 (1994).

[23] A. Fleszar, A. A. Quong, and A. G. Eguiluz, *Band-structure and many-body effects in the dynamical response of aluminum metal*, Phys. Rev. Lett. **74**, 590 (1995).

[24] J. A. Soininen and E. L. Shirley, *Scheme to calculate core hole-electron interactions in solids*, Phys. Rev. B **64**, 165112 (2001).

[25] A. G. Marinopoulos, L. Reining, V. Olevano, A. Rubio, T. Pichler, X. Liu, M. Knupfer, and J. Fink, *Anisotropy and interplane interactions in the dielectric response of graphite*, Phys. Rev. Lett. **89**, 076402 (2002).

[26] A. Marini, R. D. Sole, and A. Rubio, *Bound excitons in time-dependent density-functional theory: Optical and energy-loss spectra*, Phys. Rev. Lett. **91**, 256402 (2003).

[27] A. G. Marinopoulos, L. Reining, A. Rubio, and V. Olevano, *Ab initio study of the optical absorption and wave-vector-dependent dielectric response of graphite*, Phys. Rev. B **69**, 245419 (2004).

[28] J. A. Soininen, A. L. Ankudinov, and J. J. Rehr, *Inelastic scattering from core-electrons: a multiple scattering approach*, Phys. Rev. B **72**, 045136 (2005).

[29] A. B. Rocha and C. E. Bielschowsky, *Inner-shell excitations of water molecule*, Chem. Phys. **243**, 9 (1999).

[30] N. Durante, U. T. Lamanna, G. P. Arrighini, and C. Guidotti, *Generalized oscillator strengths of polyatomic molecules I. H_2O*, Theor. Chim. Acta **90**, 115 (1995).

[31] T. Giannerini, I. Borges Jr, and E. Hollauer, *Configuration interaction and relaxation effects on generalized and optical oscillator strengths of the H_2O molecule: The $X^1A_1 \rightarrow A^1B_1$ transition*, J. El. Spectr. Rel. Phenom. **155**, 40 (2007).

[32] N. Watanabe, D. Suzuki, and M. Takahashi, *Experimental and theoretical study on generalized oscillator strengths of the valence-shell electronic excitations in CF_4*, J. Chem. Phys **134**, 064307 (2011).

[33] K. Hämäläinen and S. Manninen, *Resonant and non-resonant inelastic x-ray scattering*, J. Phys.: Cond. Matt. **13**, 7539 (2001).

[34] M. J. Cooper, P. E. Mijnarends, N. Shiotani, N. Sakai, and A. Bansil, *X-ray Compton Scattering* (Oxford University Press, Oxford, 2004).

[35] J. W. M. DuMond, *Compton modified line structure and its relation to the electron theory of solid bodies*, Phys. Rev. **33**, 643 (1929).

[36] L. van Hove, *Correlations in space and time and born approximation scattering in systems of interacting particles*, Phys. Rev. **95**, 249 (1954).

[37] D. Pines and P. Nozières, *The Theory of Quantum Liquids* (W. A. Benjamin, Inc., New York, 1966).

[38] M. Inokuti, *Inelastic collisions of fast charged particles with atoms and molecules - the Bethe theory revisited*, Photochem. Photobiol. **44**, 279 (1986).

[39] I. Campillo, J. M. Pitarke, and A. G. Eguiluz, *Electronic stopping power of aluminum crystal*, Phys. Rev. B **58**, 10307 (1998).

[40] H. Hayashi, N. Watanabe, Y. Udagawa, and C.-C. Kao, *The complete optical spectrum of liquid water measured by inelastic x-ray scattering*, Proc. Nat. Acad. Sci. USA **97**, 6264 (2000).

[41] D. Emfietzoglou, F. A. Cucinotta, and H. Nikjoo, *A complete dielectric response model for liquid water: a solution of the Bethe ridge problem*, Radiat. Res. **164**, 202 (2005).

[42] S. Tanaka and S. Mukamel, *Coherent x-ray Raman spectroscopy: a nonlinear local probe for electronic excitations*, Phys. Rev. Lett. **89**, 043001 (2002).

[43] U. Harbola and S. Mukamel, *Coherent stimulated x-ray Raman spectroscopy: Attosecond extension of resonant inelastic x-ray Raman scattering*, Phys. Rev. B **79**, 085108 (2009).

[44] D. M. Hirst, *Potential Energy Surfaces: Molecular Structure & Reaction Dynamics* (Taylor & Francis, London, 1985).

[45] G. A. Worth and L. S. Cederbaum, *Beyond Born-Oppenheimer: Molecular dynamics through a conical intersection*, Ann. Rev. Phys. Chem. **55**, 127 (2004).

[46] E. B. Wilson, J. C. Decius, and P. C. Cross, *Molecular Vibrations: The Theory of Infrared and Raman Vibrational Spectra* (McGraw-Hill, New York, 1955).

[47] U. Hergenhahn, *Vibrational structure in inner shell photoionization of molecules*, J. Phys. B: At. Mol. Opt. Phys. **37**, R89 (2004).

[48] A. Szabo and N. S. Ostlund, *Modern Quantum Chemistry* (Dover Publications, Inc., Mineola, 1989).

[49] L. Hedin, *New method for calculating the one-particle Green's function with application to the electron gas problem*, Phys. Rev. **139**, A796 (1965).

[50] G. Onida, L. Reining, and A. Rubio, *Electronic excitations: density-functional versus many-body Green's-function approaches*, Rev. Mod. Phys. **74**, 601 (2002).

[51] P. Hohenberg and W. Kohn, *Inhomogeneous electron gas*, Phys. Rev. **136**, B864 (1964).

[52] W. Kohn and L. J. Sham, *Self-consistent equations including exchange and correlation effects*, Phys. Rev. **140**, A1133 (1965).

[53] R. O. Jones and O. Gunnarsson, *The density functional formalism, its applications and prospects*, Rev. Mod. Phys. **61**, 689 (1989).

[54] S. F. Sousa, P. A. Fernandes, and M. J. Ramos, *General performance of density functionals*, J. Phys. Chem. A **111**, 10439 (2007).

[55] J. P. Perdew, K. Burke, and M. Ernzerhof, *Generalized gradient approximation made simple*, Phys. Rev. Lett. **77**, 3865 (1996).

[56] J. Tao, J. P. Perdew, V. N. Staroverov, and G. E. Scuseria, *Climbing the density functional ladder: Nonempirical meta-generalized gradient approximation designed for molecules and solids*, Phys. Rev. Lett. **91**, 146401 (2003).

[57] A. Görling, *Exact exchange-correlation kernel for dynamic response properties and excitation energies in density-functional theory*, Phys. Rev. A **57**, 3433 (1998).

[58] J. P. Perdew and A. Zunger, *Self-interaction correction to density-functional approximations for many-electron systems*, Phys. Rev. B **23**, 5048 (1981).

[59] E. E. Dahlke and D. G. Truhlar, *Improved density functionals for water*, J. Phys. Chem. B **109**, 15677 (2005).

[60] J. P. Perdew, R. G. Parr, M. Levy, and J. L. Baldus Jr, *Density-functional theory for fractional particle number: derivative discontinuities of the energy*, Phys. Rev. Lett. **49**, 1691 (1982).

[61] A. Görling, *Density functional theory beyond the Hohenberg-Kohn theorem*, Phys. Rev. A **59**, 3359 (1999).

[62] M. Leetmaa, M. P. Ljungberg, A. Lyubartsev, A. Nilsson, and L. G. M. Pettersson, *Theoretical approximations to X-ray absorption spectroscopy of liquid water and ice*, J. El. Spectr. Rel. Phenom. **177**, 135 (2010).

[63] J. F. Janak, *Proof that $\partial E/\partial n_i = \varepsilon$ in density-functional theory*, Phys. Rev. B **18**, 7165 (1978).

[64] J. C. Slater, *Quantum Theory of Molecules and Solids* (McGraw-Hill, New York, 1974).

[65] A. Hesselmann and A. Görling, *Blindness of the exact density response function to certain types of electronic excitations: Implications for time-dependent density-functional theory*, Phys. Rev. Lett. **102**, 233003 (2009).

[66] *Time-Dependent Density Functional Theory*, edited by M. A. L. Marques, C. A. Ullrich, F. Nogueira, A. Rubio, K. Burke, and E. K. U. Gross (Springer, Heidelberg, 2004).

[67] P. Abbamonte, K. D. Finkelstein, M. D. Collins, and S. M. Gruner, *Imaging density disturbances in water with a 41.3-attosecond time resolution*, Phys. Rev. Lett **92**, 237401 (2004).

[68] E. Runge and E. K. U. Gross, *Density-functional theory for time-dependent systems*, Phys. Rev. Lett. **52**, 997 (1984).

[69] M. E. Casida, in *Recent Advances in Computational Chemistry*, edited by D. E. Chong (World Scientific, Singapore, 1995), Vol. 1.

[70] K. Yabana and G. F. Bertsch, *Time-dependent local-density approximation in real time*, Phys. Rev. B **54**, 4484 (1996).

[71] I. Vasiliev, S. Öğüt, and J. R. Chelikowsky, *Ab initio excitation spectra and collective electronic response in atoms and clusters*, Phys. Rev. Lett. **82**, 1919 (1999).

[72] H.-C. Weissker, J. Serrano, S. Huotari, F. Bruneval, F. Sottile, G. Monaco, M. Krisch, V. Olevano, and L. Reining, *Signatures of short-range many-body effects in the dielectric function of silicon for finite momentum transfer*, Phys. Rev. Lett. **97**, 237602 (2006).

[73] K. I. Igumenshchev, S. Tretiak, and V. Y. Chernyak, *Excitonic effects in a time-dependent density functional theory*, J. Chem. Phys. **127**, 114902 (2007).

[74] V. Turkowski, A. Leonardo, and C. A. Ullrich, *Time-dependent density-functional approach for exciton binding energies*, Phys. Rev. B **79**, 233201 (2009).

[75] A. Dreuw, J. L. Weisman, and M. Head-Gordon, *Long-range charge-transfer excited states in time-dependent density functional theory require non-local exchange*, J. Chem. Phys. **119**, 2943 (2003).

[76] N. T. Maitra, F. Zhang, R. J. Cave, and K. Burke, *Double excitations within time-dependent density functional theory linear response*, J. Chem. Phys. **120**, 5932 (2004).

[77] A. Wasserman, N. T. Maitra, and K. Burke, *Accurate Rydberg excitations from the local density approximation*, Phys. Rev. Lett. **91**, 263001 (2003).

[78] N. A. Besley and F. A. Asmuruf, *Time-dependent density functional theory calculations of the spectroscopy of core electrons*, Phys. Chem. Chem. Phys. **12**, 12024 (2010).

[79] Z. L. Cai, K. Sendt, and J. R. Reimers, *Failure of density-functional theory and time-dependent density-functional theory for large extended pi systems*, J. Chem. Phys **117**, 5543 (2002).

[80] M. Stener, G. Fronzoni, and M. de Simone, *Time dependent density functional theory of core electrons excitations*, Chem. Phys. Lett. **373**, 115 (2003).

[81] H. N. Y. Imamura, *Time-dependent density functional theory (TDDFT) calculations for core-excited states: Assessment of an exchange functional combining the Becke88 and van Leeuwen-Baerends-type functionals*, Chem. Phys. Lett. **419**, 297 (2006).

[82] N. V. Cohan and H. F. Hameka, *Born-Oppenheimer approximation and the calculation of infrared intensities*, J. Chem. Phys. **45**, 4392 (1966).

[83] M. Lax, *The Franck-Condon principle and its application to crystals*, J. Chem. Phys. **20**, 1752 (1952).

[84] J. Katriel, *Second quantization and the general two-centre harmonic oscillator integral*, J. Phys. B: At. Mol. Phys. **3**, 1315 (1970).

[85] M. P. de Miranda, J. A. Beswick, P. Parent, C. Laffon, G. Tourillon, A. Cassuto, G. Nicolas, and F. X. Gadea, *Fine vibrational structure in core-to-bound spectra of polyatomic molecules*, J. Chem. Phys. **101**, 5500 (1994).

[86] S. Y. Lee and E. J. Heller, *Time-dependent theory of Raman scattering*, J. Chem. Phys. **71**, 4777 (1979).

[87] C. Zhu, K. K. Liang, M. Hayashi, and S. H. Lin, *Theoretical treatment of anharmonic effect on molecular absorption, fluorescence spectra, and electron transfer*, Chem. Phys. **358**, 137 (2009).

[88] R. M. Martin, *Electronic Structure: Basic Theory and Practical Methods* (Cambridge University Press, Cambridge, 2004).

[89] J. R. Chelikowsky, N. Troullier, and Y. Saad, *Finite-difference-pseudopotential method: Electronic structure calculations without a basis*, Phys. Rev. Lett. **72**, 1240 (1994).

[90] T. L. Beck, *Real-space mesh techniques in density-functional theory*, Rev. Mod. Phys. **72**, 1041 (2000).

[91] A. Castro, H. Appel, M. Oliveira, C. A. Rozzi, X. Andrade, F. Lorenzen, M. A. L. Marques, E. K. U. Gross, and A. Rubio, *Octopus: a tool for the application of time-dependent density functional theory*, Phys. Stat. Sol. B **243**, 2465 (2006).

[92] J. Enkovaara, C. Rostgaard, J. J. Mortensen, J. Chen, M. Dulak, L. Ferrighi, J. Gavnholt, C. Glinsvad, V. Haikola, H. A. Hansen, H. H. Kristoffersen, M. Kuisma, A. H. Larsen, L. Lehtovaara, M. Ljungberg, O. Lopez-Acevedo, P. G. Moses, J. Ojanen, T. Olsen, V. Petzold, N. A. Romero, J. Stausholm-Mller, M. Strange, G. A. Tritsaris, M. Vanin, M. Walter, B. Hammer, H. Häkkinen, G. K. H. Madsen, R. M. Nieminen, J. K. Nørskov, M. Puska, T. T. Rantala, J. Schitz, K. S. Thygesen, and K. W. Jacobsen, *Electronic structure calculations with GPAW: a real-space implementation of the projector augmented-wave method*, J. Phys.: Cond. Matt. **22**, 253202 (2010).

[93] S. R. White, J. W. Wilkins, and M. P. Teter, *Finite-element method for electronic structure*, Phys. Rev. B **39**, 5819 (1989).

[94] L. Lehtovaara, V. Havu, and M. Puska, *All-electron density functional theory and time-dependent density functional theory with high-order finite elements*, J. Chem. Phys. **131**, 054103 (2009).

[95] K. Hermann, L. G. M. Pettersson, M. E. Casida, C. Daul, A. Goursot, A. Koester, E. Proynov, A. St-Amant, D. R. Salahub, V. Carravetta, H. Duarte, C. Friedrich, N. Godbout, J. Guan, C. Jamorski, M. Lebouf, M. Leetmaa, M. Nyberg, S. Patchkovskii, L. Pedocchi, F. Sim, L. Triguero, and A. Vela, 2009, StoBe-deMon version 3.0 (http://www.rz-berlin.mpg.de/∼hermann/StoBe).

[96] L. Triguero, L. G. M. Pettersson, and H. Ågren, *Calculations of near-edge x-ray-absorption spectra of gas-phase and chemisorbed molecules by means of density-functional and transition-potential theory*, Phys. Rev. B **58**, 8097 (1998).

[97] Octopus computer code (http://www.tddft.org/programs/octopus).

[98] M. A. L. Marques, A. Castro, A. Castro, G. F. Bertsch, and A. Rubio, *Octopus: a first-principles tool for excited electron-ion dynamics*, Comput. Phys. Commun. **151**, 60 (2003).

[99] C. R. Natoli, M. Benfatto, S. D. Longa, and K. Hatada, *X-ray absorption spectroscopy: State-of-the-art analysis*, J. Synch. Rad. **10**, 26 (2003).

[100] P. A. Lee and G. Beni, *New method for the calculation of atomic phase shifts: Application to extended x-ray absorption fine structure (EXAFS) in molecules and crystals*, Phys. Rev. B **15**, 2862 (1977).

[101] U. von Barth and G. Grossmann, *Static and dynamical effects of core holes in KLV Auger, SXE, and SXA spectra of simple metals*, Physica Scripta **28**, 107 (1983).

[102] M. Nyberg, Y. Luo, L. Triguero, L. G. M. Pettersson, and H. Ågren, *Core-hole effects in x-ray absorption spectroscopy*, Phys. Rev. B **60**, 7956 (1999).

[103] B. Hetnyi, F. D. Angelis, P. Giannozzi, and R. Car, *Calculation of near-edge x-ray-absorption fine structure at finite temperatures: Spectral signatures of hydrogen bond breaking in liquid water*, J. Chem. Phys. **120**, 8632 (2004).

[104] M. Cavalleri, M. Odelius, D. Nordlund, A. Nilsson, and L. G. M. Pettersson, *Half or full core hole in density functional theory X-ray absorption spectrum calculations of water*, Phys. Chem. Chem. Phys. **7**, 2854 (2005).

[105] J. D. Smith, C. D. Cappa, B. M. Messer, W. S. Drisdell, R. C. Cohen, and R. J. Saykally, *Probing the local structure of liquid water by x-ray absorption spectroscopy*, J. Phys. Chem. B **110**, 20038 (2006).

[106] V. Bonifacic and S. Huzinaga, *Atomic and molecular calculations with the model potential method. I*, J. Chem. Phys. **60**, 2779 (1974).

[107] L. G. M. Pettersson, U. Wahlgren, and O. Gropen, *Effective core potential parameters for first- and second-row atoms*, J. Chem. Phys. **86**, 2176 (1987).

[108] M. Petersilka, U. J. Gossmann, and E. K. U. Gross, *Excitation energies from time-dependent density-functional theory*, Phys. Rev. Lett. **76**, 1212 (1996).

[109] A. Castro, M. A. L. Marques, and A. Rubio, *Propagators for the time-dependent Kohn-Sham equations*, J. Chem. Phys **121**, 3425 (2004).

[110] W. E. Pickett, *Pseudopotential methods in condensed matter applications*, Comput. Phys. Rep. **9**, 115 (1989).

[111] F. Gygi and G. Galli, *Real-space adaptive-coordinate electronic-structure calculations*, Phys. Rev. B **52**, R2229 (1995).

[112] T. L. Beck, *Multigrid high-order mesh refinement techniques for composite grid electrostatics calculations*, J. Comput. Chem. **20**, 1731 (1999).

[113] M. Walter, H. Häkkinen, L. Lehtovaara, M. Puska, J. Enkovaara, C. Rostgaard, and J. J. Mortensen, *Time-dependent density-functional theory in the projector augmented-wave method*, J. Chem. Phys **128**, 244101 (2008).

[114] L. Koponen, L. Tunturivuori, M. J. Puska, and R. M. Nieminen, *Photoabsorption spectra of boron nitride fullerenelike structures*, J. Chem. Phys. **126**, 214306 (2007).

[115] X. Andrade, A. Castro, D. Zueco, J. L. Alonso, P. Echenique, F. Falceto, and A. Rubio, *Modified Ehrenfest formalism for efficient large-scale ab initio molecular dynamics*, J. Chem. Theory Comput. **5**, 728 (2009).

[116] Y. Takimoto, F. D. Vila, and J. J. Rehr, *Real time time-dependent density functional theory approach for frequency-dependent non-linear optical response in photonic molecules*, J. Chem. Phys. **127**, 154114 (2007).

[117] J. L. Alonso, X. Andrade, P. Echenique, F. Falceto, D. Prada-Gracia, and A. Rubio, *Efficient formalism for large-scale ab initio molecular dynamics based on time-dependent density functional theory*, Phys. Rev. Lett. **101**, 96403 (2008).

[118] T. Nakatsukasa and K. Yabana, *Photoabsorption spectra in the continuum of molecules and atomic clusters*, J. Chem. Phys. **114**, 2550 (2001).

[119] C. L. Cheng, J. S. Evans, and T. Van Voorhis, *Simulating molecular conductance using real-time density functional theory*, Phys. Rev. B **74**, 155122 (2006).

[120] G. F. Bertsch, J.-I. Iwata, A. Rubio, and K. Yabana, *Real-space, real-time method for the dielectric function*, Phys. Rev. B **62**, 7998 (2000).

[121] A. Hohl, T. Wieder, O. A. van Aken, T. E. Weirich, G. Denninger, M. Vidal, S. Oswald, C. Deneke, J. Mayer, and H. Fuess, *An interface clusters mixture model for the structure of amorphous silicon monoxide (SiO)*, J. Non-Cryst. Solids **320**, 255 (2003).

[122] D. König, J. Rudd, M. A. Green, and G. Conibeer, *Role of the interface for the electronic structure of Si quantum dots*, Phys. Rev. B **78**, 035339 (2008).

[123] H. Sternemann, C. Sternemann, G. T. Seidler, T. T. Fister, A. Sakko, and M. Tolan, *An extraction algorithm for core-level excitations in non-resonant inelastic X-ray scattering spectra*, J. Synch. Rad. **15**, 162 (2008).

[124] T. Pylkkänen, J. Lehtola, M. Hakala, A. Sakko, G. Monaco, S. Huotari, and K. Hämäläinen, *Universal signature of hydrogen bonding in the oxygen K-edge spectrum of alcohols*, J. Phys. Chem. B **114**, 13076 (2010).